# Nonsteady Plume-Wall Interactions in Rocket Launch Tubes

M. J. Marongiu,* H. H. Korst,† and R. A. White‡
*University of Illinois at Urbana-Champaign, Urbana, Illinois*

**Strong and potentially destructive pressure amplitudes have been observed during the early stages of rocket launch from canisters. This can be explained by a traveling wave system that is caused by quasiperiodic changes in irreversibility levels between the critical flow conditions in the rocket nozzle and at the exit of the launch tube. The interaction between the wave system and the wake region near the base of the rocket and its controlling flow mechanisms result in the complex nonsteady overall interaction of supersonic and subsonic flow regions. Observations by means of the hydraulic analogy allow the identification of constituent mechanisms, which are subsequently subjected to a highly simplified analysis and finally compared to experimental results under laboratory conditions. General agreement between theoretical and experimental results (pressure amplitudes and frequencies) support the validity of the proposed analytical approach.**

## Nomenclature

$A$ = area, m
$c$ = acoustic velocity, m-s$^{-1}$
$D$ = channel height or diameter, m
$f$ = frequency, Hz
$H$ = backstep height, m
$L$ = channel length, m
$m$ = mass flow rate, kg $- s^{-1}$ (per unit width)
$P$ = absolute pressure, N-m$^{-2}$
$R$ = gas constant, N-m-K$^{-1}$ kg$^{-1}$; radius, m
$S$ = moving shock velocity, m-s$^{-1}$
$t$ = time, s
$t_o$ = base time constant, $t_o = h/c_{o1}$, s
$T$ = absolute temperature, K
$v_R$ = velocity of rocket
$W$ = test-section width, m
$x,X$ = streamwise coordinate or distance, m
$\theta$ = streamline angle, radians
$\rho$ = density, kg-m$^{-3}$
$\omega$ = Prandtl-Meyer expansion angle, radians

*Dimensionless Quantities*

$C$ = Crocco number, $U/U_{\max}$
$C_e$ = effective area ratio coefficient
$k$ = specific heat ratio
$M$ = Mach number
$\phi$ = velocity ratio (further specified in text)
$\sigma$ = jet spread rate parameter
$\tau$ = dimensionless time

*Subscripts*

$I$ = conditions in primary nozzle
$II$ = conditions in secondary nozzle
$b$ = base region
$c$ = channel region
$d$ = discriminating or stagnating streamline
$e$ = nozzle exit plane
$j$ = zero streamline or jet streamline
$v$ = wake travel time
$w$ = conditions prevailing in the wave region
$x$ = normal shock wave conditions before wave
$y$ = normal shock wave conditions after wave
0 = stagnation conditions

*Superscript*

* = critical conditions

Presented as Paper 87-1601 at the AIAA 22nd Thermophysics Conference, Honolulu, HI, June 8-10, 1987; received June 25, 1987; revision received Jan. 19, 1988. 

*Visiting Research Associate.
†Professor Emeritus. Fellow AIAA.
‡Professor. Associate Fellow AIAA.

## I. Introduction

PROPULSIVE jets emerging from underexpanded convergent or convergent-divergent nozzles form plumes that commonly interfere with solid or hydrodynamic (slipstream) boundaries.[1,2] For certain configurations, impingements between the slipstream and solid boundaries can produce nonsteady flowfields characterized by the appearance of transient, large-amplitude pressure wave systems.[3] The study of wake regions bounded by mixing layers and controlled by their mass entrainment and reattachment mechanisms have been the subject of intensive research for several decades. Such work has included experimental, analytical, and computational approaches in attempts to explain and predict the characteristics of these complex flowfields. Flow component models[1] have been particularly useful in delineating the controlling mechanisms for such complex flows under steady, or quasisteady, operating conditions.

Nonsteady flowfields may occur when the jet flow encounters a constriction downstream in which critical flow conditions have to be satisfied leading to temporary mass storage requirements between critical cross sections. Rockwell[4] has enumerated and classified a variety of these cases exhibiting nonsteady phenomena, some of which had been previously investigated experimentally.[5-8] Such nonsteady interactions have been observed during the early phases of in-tube launch of rockets or missiles, often accompanied by strong, and possibly destructive, pressure wave buildup in the canister.

This paper develops criteria for the appearance of such nonsteady operational modes and their analysis by 1) delineation of flow components, and 2) their subsequent synthesis into an overall model for cyclic performance. Because of the complex nature of the various flow components and their interaction, the analysis of the problem, by necessity, requires far-reaching simplifications in treatment. Support for the validity of such abstractions is furnished by experimental evidence of two kinds, namely, 1) qualitative observations of the overall systems performance by means of the hydraulic analogy (water table), and 2) quantitative studies with high-velocity air flows of both component mechanisms[9] and entire systems in cyclic modes of operation. The experimental evidence, although validating the basic analysis, also points to the difficulties in separating individual flow mechanisms with respect to their exact location in space and time.

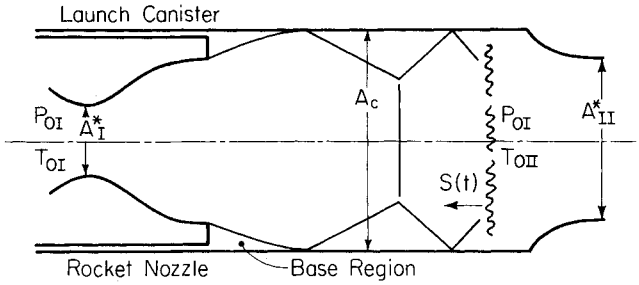


**Fig. 1 Typical plume-wall interactions during the initial launch phases of rockets [$S(t)$ is needed to account for mass storage between the moving shock system and second critical cross section].**

## II. Flow Model

A simple but representative configuration that lends itself to a study of the phenomenon is shown in Fig. 1. It is composed of a converging-diverging nozzle, operating with critical flow in the first throat $A^*_I$, which discharges into a smooth channel of larger but uniform cross section. The channel (launch tube) may end with a constrictor nozzle $A^*_{II}$, or without an area reduction. Either type of exit condition can give rise to critical flow conditions, depending on the geometry, rocket-chamber to ambient-pressure ratio, and the dissipative mechanisms occurring in the system. If critical flow rates in the first (rocket nozzle) throat and the (effective) second throat do not match, mass discharge or storage will be required in the launch tube. In the absence of sufficiently high missile velocity in the early launch phases but sufficient distance between the nozzle exit and the launcher exit to allow plume impingement on the wall, a nonsteady wave system may appear and interfere with the dissipative mechanism in the base region, along the tube walls, and within the tube itself. This can change the dissipative flow components sufficiently to produce a cyclic mode of operation.

Because of the complex nature of the problem it was necessary to seek guidance in the form of preliminary experiments by using the hydraulic analogy (water table). Diagnostic experiments with high-velocity airflow in channels representing individual flow mechanisms and overall system behavior were also undertaken to provide understanding and support for the theoretical analysis.

### Preliminary Water Table Experiments

Use of the hydraulic analogy in the study of nonsteady flow processes takes advantage of the vastly extended time scale, which in the present case is of the order of 5000:1, as compared to air-channel flow experiments. This coupled with the ease of flow visualization makes the hydraulic analogy a very attractive and useful tool. Figure 2 is a sequence of photographs showing flow patterns referring to the instantaneous flow conditions, as indicated in Fig. 3.

Based on the observations of the water table experiments (again see Figs. 2 and 3), the following mechanisms can be identified:

1) The fully developed wake (base pressure) establishes supersonic flow in the channel. The presence of a second critical cross section requires a shock system to satisfy subsonic approaching flow.

2) If the strength of such a shock system together with the wall friction in the channel produces irreversibilities sufficiently strong that the second throat is not large enough to discharge the mass rate supplied by the primary nozzle, then mass has to be stored in the channel, forcing the shock system to move upstream.

3) During the upstream motion of the shock system, the rate of dissipation is modified as the supersonic region of the channel flow is decreasing. This is reflected by a change in strength and speed of the wave.

4) As the wave system approaches and interferes with the wake at the primary nozzle exit, the shear layer bounding the

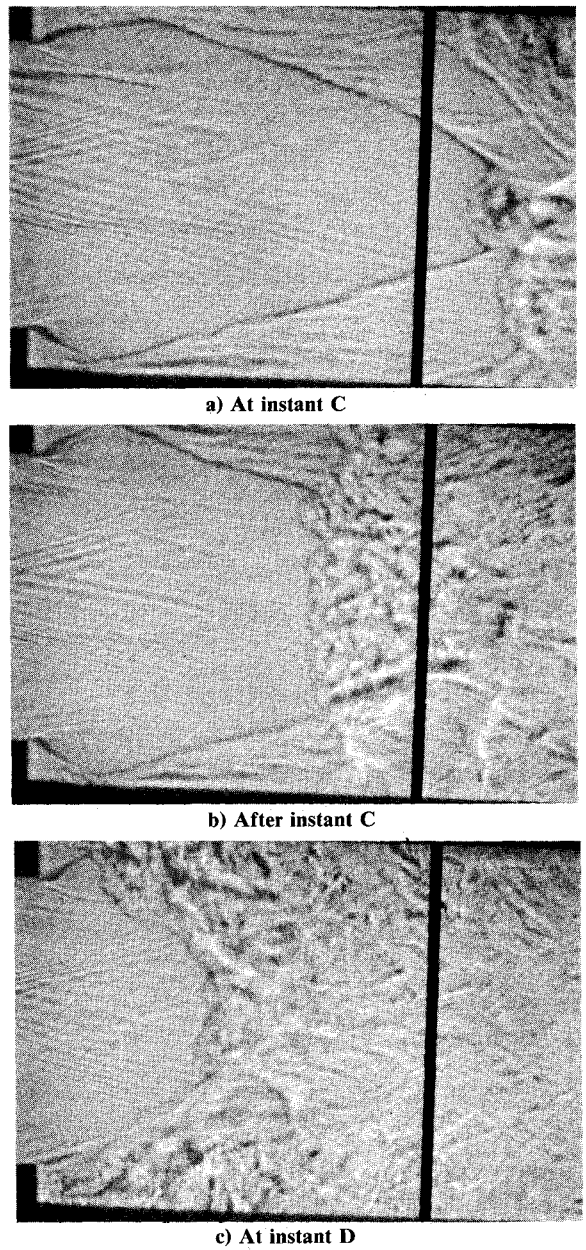

a) At instant C

b) After instant C

c) At instant D

**Fig. 2 Water table photographs showing the instantaneous flowfield at various times in a typical cycle (instants refer to time markers in Fig. 3).**

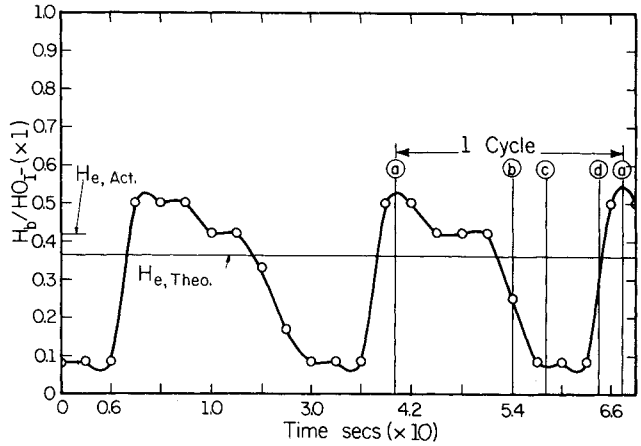


**Fig. 3 Base area water height ($H_b$) vs time on the water table model during nonsteady operation (all $H$ values in this figure refer to water heights).**

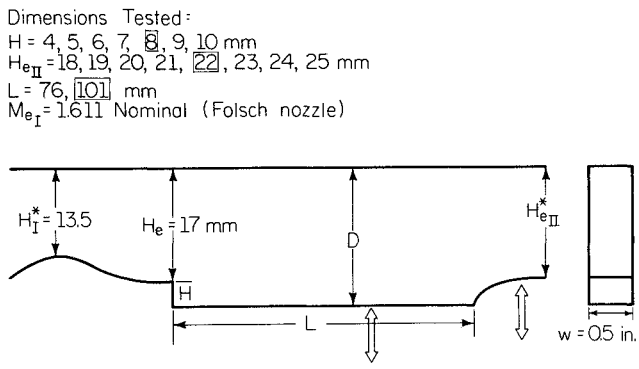


**Fig. 4 Two-dimensional configuration for diagnostic experiments showing the dimensions tested.**

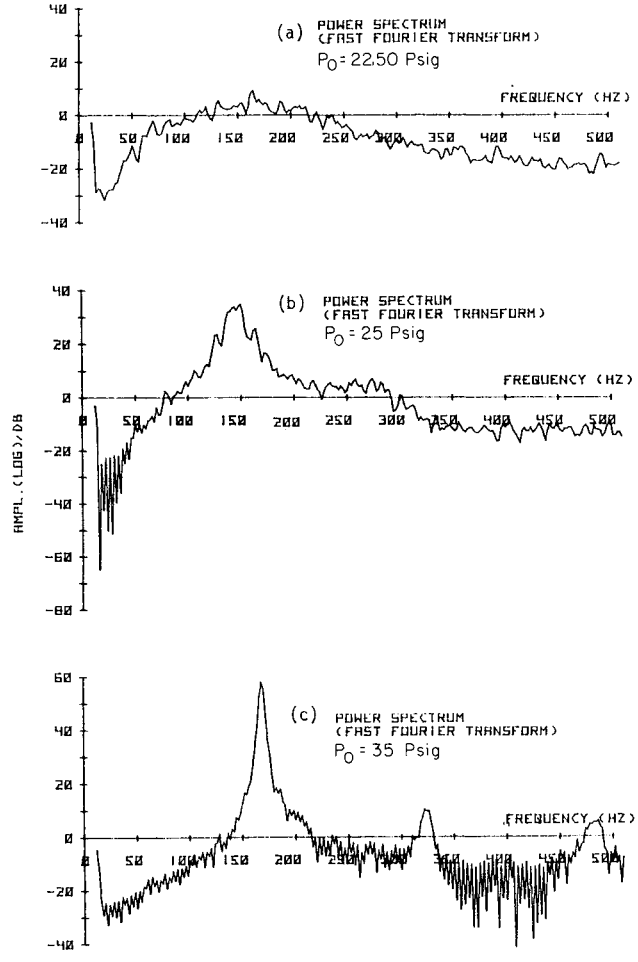


**Fig. 5 Power spectra of base pressure oscillations for: a) $L$ = 101 mm, $P_{o_I}$ = 22.5 psig; b) $L$ = 101 mm, $P_{o_I}$ = 25 psig; and c) $L$ = 101 mm, $P_{o_I}$ = 35 psig.**

wake will detach from the wall, and the base pressure will increase toward the exit pressure of the nozzle. Under these conditions the level of irreversibilities in the channel is drastically reduced, and the rate of outflow through the second critical cross section increases so that the stored mass may be discharged.

5) The free-mixing layer along the surface of the jet discharging from the nozzle begins to entrain mass so that a new wake will be generated, and the original base pressure is restored.

Although this sequence of events can be conveniently observed with the help of the hydraulic analogy, a theoretical analysis is, in view of the complexity of the flow patterns, dependent on sweeping simplifications.

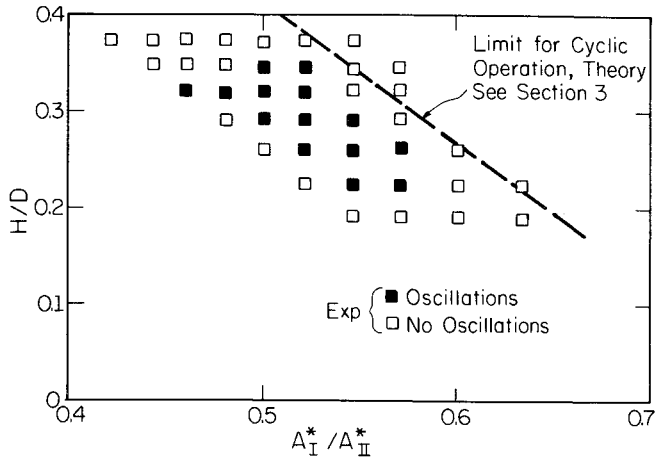


**Fig. 6 Influence of geometrical parameters on the base pressure oscillations in two-dimensional channels of the type shown in Fig. 4.**

**Table 1 Analytical concepts as applied to the flow components**

| No. components | Analytical concepts: Steady 1-D | Quasisteady 1-D | Quasisteady 2-D | Nonsteady 1-D |
|---|---|---|---|---|
| 1) Primary nozzle flow | X | | | |
| 2) Viscous entrainment along wake | | | X | |
| 3) Sudden expansion and frictional channel flow | | X | | |
| 4) Choking in second throat | | X | | |
| 5) Time-dependent mass storage | | | | X |
| 6) Shock (wave) kinematics and dynamics | | | | X |
| 7) Shock-wave interaction | | | X | |
| 8) Mass discharge at second throat | | X | | |
| 9) Wake pumpdown at nozzle base | | | X | |

### Diagnostic Experiments in Air Channels

In order to establish conditions producing nonsteady operation, a two-dimensional channel of constant width was constructed with provisions for varying the pertinent geometries (base-step height, second-throat height, and channel length) while leaving the primary nozzle exit height constant (see Fig. 4). Shown in Fig. 5 (power spectrum of base pressure) is the gradual onset of cyclic oscillations as the primary nozzle pressure is increased, and critical flow conditions are produced in the second throat. Similar results have been obtained for other geometries. The effect of the critical area ratios $A_I^*/A_{II}^*$ and the base-to-channel height ratio on the occurrence of oscillations is demonstrated in Fig. 6. Based on the above observations, it is possible to propose a theoretical flow model as described below.

### Flow Model Components

Here, flow components are delineated for subsequent synthesis into an overall operational model. The components are identified as follows: 1) the primary nozzle flow, 2) viscous entrainment along the separated flow (base) region, 3) the abrupt expansion at the nozzle base and frictional channel flow, 4) choking in the second throat, 5) a time-dependent mass storage mechanism, 6) shock system (wave kinematics

and dynamics, 7) shock interaction with the wake and resulting reduction in level of downstream dissipation, 8) mass discharge through the second throat, and 9) pump-down of the wake at the base of the nozzle. The treatment of these flow processes fall into four categories, each of which may be applicable to one or more components, as shown in Table 1. Since the nonsteady nature of the problem is linked to the modification of the dissipation levels due to shock-wake interaction, the analysis of the shock kinematics and dynamics is of utmost importance.

Although the wave system is of a highly complicated structure, it is fortuitous that the Mach number level of the supersonic flow over which the compression waves have to travel is high enough so that the subsonic flowfield behind the shock system can be treated as effectively one-dimensional.[10] In the following section, the major flow components are discussed individually.

## III. Theoretical Analysis

### Sudden Expansion to Supersonic Channel Flow

The jet discharging from the nozzle undergoes an adjustment to channel flow that is treated as producing one-dimensional, supersonic flow at the end of the wake. Because of the sudden enlargement in cross section and a prevailing base pressure $P_b$, this process will be irreversible and results in an increase in entropy, and being adiabatic, a decrease in stagnation pressure. (It must be noted that this requirement of the second law imposes an upper limit on the value of the base pressure). Utilizing the fundamental conservation principles for mass and momentum, together with simple adiabatic conditions, the one-dimensional supersonic flow downstream of the wake is determined.

### Channel Flow

Fanno-type flow starts at the end of the wake, and the friction coefficient is determined on the basis of an equivalent diameter concept (considering Reynolds number and absolute wall roughness). This friction coefficient is subsequently adopted for the subsonic portion of the channel flow, which is permissible because of the relatively small changes in entropy downstream of the moving shock.

### Wave System

A left-running normal shock is needed to allow for mass storage in the channel if the flow irreversibilities cause the second critical cross section to choke at a lesser mass rate than that delivered by the primary nozzle. Denoting the absolute velocity of the shock front by $S$, the mass storage condition is expressed by

$$m_I^* - m_{II}^* = S(\rho_y - \rho_x)A_c \tag{1}$$

where $\rho_y$ and $\rho_x$ are the densities downstream and upstream, respectively, of the (moving) normal shock.

In terms of the geometrical and flow parameters, one now expresses the dimensionless shock speed as

$$\frac{S}{c_o} = \left(\frac{2}{k+1}\right)^{k+1/2(k-1)} \left\{ A_I^* \frac{P_{o_I}}{T_{o_I}} \left[ 1 - \frac{AII}{A_I^*} \frac{P_{o_{II}}}{T_{o_I}} \times \left(\frac{T_{o_I}}{T_{o_{II}}}\right)^{1/2} \right] \Big/ \frac{P_x}{T_x}\left(\frac{P_y T_x}{P_x T_y} - 1\right) A_c \right\} \tag{2}$$

where $P_{o_{II}}$ and $T_{o_{II}}$ refer to the stagnation state just upstream of the secondary critical cross section, and $P_x$, $T_x$, $P_y$, $T_y$ are determined by the strength of the moving shock $M_x$. One notes that

$$M_x = M(X) - S/c_x \tag{3}$$

and $M(X)$ is the local (supersonic) Mach number in the channel just ahead of the moving shock where the local speed of sound $c_x = c_o(T_x/T_{o_I})^{1/2}$. Also, although the entire flow system is adiabatic, $T_{o_{II}} \neq T_{o_I}$ due to the motion of the shock.

An iterative procedure is required for solving the system of Eqs. (2) and (3), and the normal shock relations. Since the absolute shock speed $S$ is much smaller than the speed of sound, a computer-based numerical solution rapidly converges.

**Table 2 I/0 for analysis of components 3 and 6 of Table 1**

```
Fanno line, supersonic/subsonic flow with moving shock
After sudden enlargement in cross section, HHK 04/01/82
2-D geometry, linear area ratios
Equivalent pipe diameter = 4*H*B/(2H + 2B), channel
Adiabatic compressible channel flow
Airflow

Stagnation temperature (deg C) = 20
Gas constant = 286.9175 Gamma = 1.4 Abs. temp. (deg R) = 273
H, throat = 0.0135 H0, Exit = 0.017 H1, channel = 0.025 H2,
  Width = 0.0127 Length, ch. = 0.101

Effective second-throat height (m) = 0.02
Stagnation pressure P0 (Pa) = 325000
Primary nozzle area ratio = 1.259259
Channel: equivalent diameter = 0.0168435 Length (m) = 0.101
Absolute roughness (mm) = 0.002
Relative roughness = 1.187402E-04

Base pressure ratio P,b/P,e = 0.55
Note that the Second Law imposes an upper limit on the
  one-dimensional interpretation of a supersonic flow
  adjustment after an abrupt expansion

Supersonic solution
Gamma = 1.4 A/A* = 1.259259
M = 1.611092
P/P0, exit = 0.2314324
Base pressure ratio P,b/P,0 = 0.1272878
M1 = 2.013775 P1 = 0.1153115 P1(Pa) = 37476.25
  P1, SUP/P0 = 0.9217989
Theta, E = 0.265088 Theta, 8 = 0.4616662
Expansion angle (deg) = 11.2631
Attachment distance = 1.607957E-02
Reynolds no. = 6962126 Friction factor = 0.0126567

Next shock location
Shock location at x = 6.698183E-02
  L = 5.090226E-02 MF = 1.88895 Local pressure P/P0 = 0.126378
Local stagnation pressure ratio P0,L/P0 = 0.8324878
Wave Mach number ( + if upstream) = 5.050253E-02
Subsonic Fanno line after normal (moving) shock
After normal shock, P/P,0 = 0.5330178 M,Y = 0.5882898
  M2 = 0.5495359
Stagnation pressure ratio = 0.6544596
Stagnation temp. ratio = 1.013727
At the end of the channel, Mach no. = 0.5539867
Stagnation pressure ratio = 0.6510074
```

Shown in Table 2 is the input-output (I/O) printout of an IBM-PC program for the geometric and flow parameters listed. It should be noted that the selection of a flow coefficient for the second throat is required (here $c_e \sim 0.9$). Inspection of the subsonic approach Mach number to the second throat, together with the geometric contraction ratio $A_{II}^*/A_c$, is in direct support of the chosen value and which accounts for the nonuniformities of the flow in the second throat. Shown in Fig. 7 are the dimensionless shock velocities $S/c_o$ for the test-section configuration, as highlighted in Fig. 4, for parametric values of $P_b/P_e$. A decrease in the absolute shock velocity is noted as the shock proceeds upstream. The relationship between momentary shock location and stagnation pressure distribution in the channel is shown in Fig. 8.

These computer results are obtained for nominal theoretical conditions as would be resulting from the channel geometry and stagnation conditions upstream of the primary nozzle. It remains to be seen what distinctive differences will be ob-

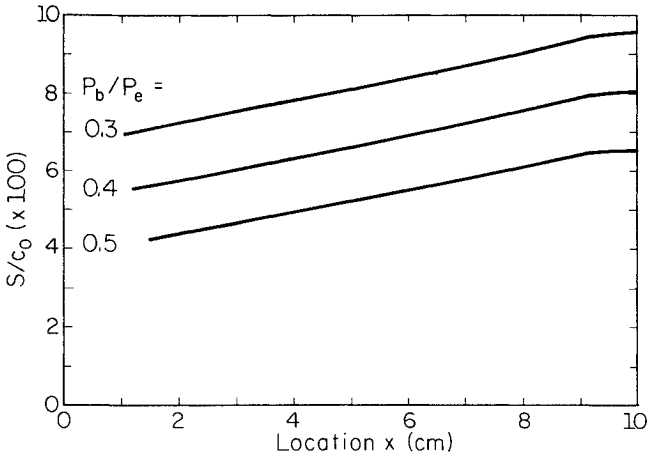


**Fig. 7 Upstream dimensionless shock wave velocity.**

served between these underlying assumptions and the actual processes involved.

**Wake Pressure History**

The process of shock wave formation and upstream motion is started by selection of a base pressure ratio $P_b/P_e$ (used as a parameter in Fig. 7) for the closed wake. Considering the base pressure development as the result of mass entrainment by the mixing region between the jet boundary and the wall, one can determine both the steady-state base pressure and the pulldown time. For the present case, a quasisteady treatment[11] is acceptable. Although calculations were originally carried out with computer programs capable of dealing with transitional, nonsimilar mixing profiles to allow the assessment of the approaching shear layer influence,[9] a simplified approach was found to be sufficient for estimating this effect. The wake evacuation process relates the rate of change of mass contained in the base region (due to change in pressure $P_w$ and wake shape (see Fig. 9a), which can be expressed as

$$\frac{dm_w}{dt} = \frac{H^2}{2}\left[\frac{d\rho_w}{dt}\cot\theta + \rho_w\frac{d(\cos\theta)}{dt}\right] \tag{4}$$

where $\rho_w = P_w(t)/RT_{o_I}$ and $P_w/P_{o_I} = [1 + (k-1)M^2(t)/2]^{k/1-k}$ and $\theta = \omega[M(t)] - \omega(M_E)$ with $\omega = \omega(M)$ the Prandtl-Meyer angle. The outflow of mass from the wake due to viscous entrainment along the wake boundary mixing region (approximated by a linear similarity profile, Fig. 9b) is given by

$$\frac{dm_w}{dt} = -\left(\frac{1}{2C^2}\right)\ell_n\left(\frac{1-\phi_j^2C^2}{1-\phi_d^2C^2}\right)(1-C^2) \times M(t)\left(1+\frac{k-1}{2}M^2\right)^{1/2}\left(\frac{k}{RT_{o_I}}\right)^{1/2} P_w\frac{H}{\sigma\sin\theta} \tag{5}$$

where $C^2 = M^2/\{[2/(k-1)] + M^2\}$, $M = M(t)$, and $\sigma$ is the empirical mixing spread parameter related to $M(t)$ by $\sigma \simeq 12 + 2.76\,M(t)$. The velocity ratio for the zero streamline is

$$\phi_j = \left\{1-(1-C^2)\exp\left[\log\left(\frac{1+C}{1-C}\right)/C - 2\right]\right\}^{1/2}/C \tag{6}$$

The velocity ratio for the stagnating streamline (neglecting the correction for incomplete turning of the freestream near reattachment[12,13]), which here compensates for neglecting the effects of finite boundary-layer thickness and sublayer transition,[14] will be

$$\phi_d = [1-(M_e/M)^2]^{1/2} \tag{7}$$

Since all variables can be expressed in terms of the Prandtl-Meyer angle $\omega(t)$, the system of Eqs. (4-7) can be solved for given values of $k$ and $M_e$ as a function of the dimensionless independent variable $\tau = t/t_o$ where the reference time is

$$t_o = H/(kRT_{o_I})^{1/2} \tag{8}$$

Shown in Fig. 10 is the solution for $k = 1.4$, $M_{1e} = 1.611$ and for conditions consistent with the shock wave motion analysis, air, $H = 0.008$ m, $T_{o_I} = 293$ K. It is of interest to note that an asymptotic value of $P_w/P_e = 0.55$ is reached, which agrees well with the measured level of the lowest base pressure. Also

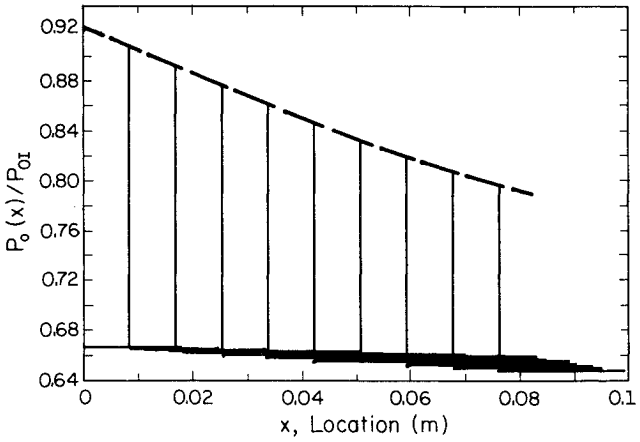


**Fig. 8 Dissipation levels in channel as a function of shock wave position in channel.**

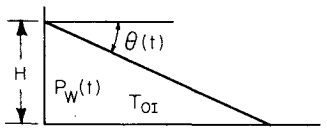


**Fig. 9a Wake evacuation components.**

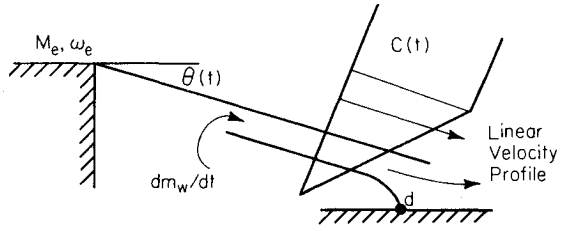


**Fig. 9b Base pressure history during wake pumpdown (same operating conditions as Fig. 5).**

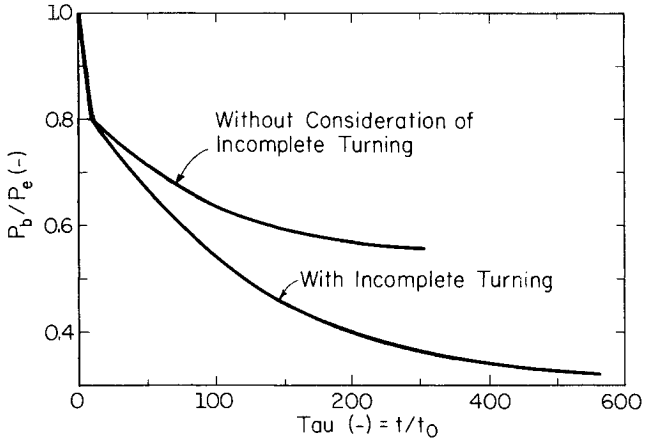


**Fig. 10 Wake evacuation history using linear similarity profiles.**

shown is the wake evacuation history for similarity profile mixing, but with consideration of incomplete turning of the freestream. Both the more detailed theoretical calculations[9] and the experimental evidence confirm the expectation that the wake evacuation will be characterized in the present case where $c_o \approx 343$ m/s, and $H = 0.008$ m, by a value of $\tau \simeq 100$.

**Component Synthesis**

The different flow mechanisms that have been treated separately can actually occur within overlapping time spans. This will be reflected by discrepancies between theoretical and experimental results, as will be discussed later.

Of importance, however, are some observations made based on the hydraulic analogy studies:

1) Within a full cycle, the time requirements for upstream motion of the wave system together with the wake pulldown appear to dominate.

2) The wave system forms somewhat upstream of the second throat (a distance approximately equal to $A_{II}^*$ [see Eq. (9)]), as should be expected considering the pattern of streamlines ahead of a constriction.

3) Pulldown of the wake in its final stages is simultaneous with the expulsion of the stored mass, so that the latter process seemingly does not have to be allowed specific time within the cycle.

4) When the wave system reaches the end of the wake, the penetration of the high pressure behind the shock into the wake is rapid and produces nearly parallel outflow from the primary nozzle, so that a new pulldown of the wake will again start.

In addition, the analytical treatment of the dissipation mechanisms leading to imbalance between critical mass flow rates in the primary and secondary throats has shown that: 1) the nonacoustic nature of the wave system kinematics exemplified by large pressure amplitudes and high relative shock front velocities capable of traveling upstream against the supersonic flowfield, 2) the low absolute shock wave velocities during the upstream travel together with evacuation times establish representative time scales for the cyclic operation, and 3) the slow absolute propagation velocity of the shock wave allows the prediction of the geometrical and operational parameters for which cyclic system performance can be expected (Fig. 6). As can be expected by inspection of the schematic flow pattern of Fig. 1, the component treatment must have serious shortcomings with respect to channel length scales. Indeed, the treatment of the shock system by lumping its dissipative mechanisms into a normal shock front, although representative for flow conditions produced near the end of the channel, lacks realism as increasing mass storage pushes the entire pattern upstream.

Because of these factors, the analysis can only provide reasonable information on peak pressures, but remains somewhat speculative with respect to cycle frequencies even though it establishes a plausible time scale. It is here suggested that a reasonable estimate for cycle frequencies can be based on the following scheme: 1) one selects an effective channel length

$$L_{\text{eff}} = L_c - H\cot\theta - A_{II}^* \tag{9}$$

for determining a dimensionless wave travel time

$$\Delta\tau_V = \Delta t_V / c_o = L_{\text{eff}}/(S/c_o) \tag{10}$$

(from Wave System section), 2) using the dimensionless wake evacuation time $\Delta\tau_w = \Delta t_w c_o/H$ (from Wake Pressure History section), and 3) considering only these two contributing time increments, the cycle frequency should be of the order of

$$f = c_o/\{[L_{\text{eff}}/(S/c_o)] + H\,\Delta\tau_w\} \tag{11}$$

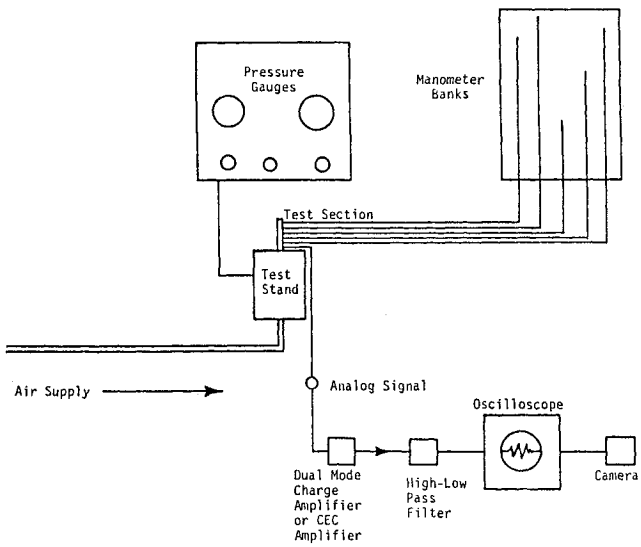


**Fig. 11 Data acquisition flow diagram for channel pressure history experiments.**

## IV. Experimental Program

The experimental program had several purposes. First, it was necessary to determine those geometrical and operational parameters that clearly cause unsteady operation. In all the experiments, unsteady flow means the occurrence of large, periodical pressure changes in the system, characterized and accompanied by base pressure oscillations. Second, it was important to have channel and base time-dependent static and stagnation pressure data to allow for corroboration of the theoretical models and a deeper understanding of the unsteady phenomena. Finally, one needed base pressure pulldown times data in order to obtain time and pressure scales of the important item-dependent fluidic entrainment mechanisms.

**Diagnostic Experiments – Water Table**

The most useful information resulted from detailed, exhaustive observations of the cyclic operations at different parametric conditions. These observations were recorded in the form of comments, drawings, sketches, still photographs, moving pictures, and videotapes.

**Two-Dimensional Airflow Experiments**

The geometrical parameters studied were (see Fig. 4) backstep height $H$, channel length $L$, channel height $D$, the secondary nozzle throat $A_{II}^*$, and the primary nozzle throat $A_I^*$. The operational parameters included only plenum stagnation pressure because facilities for back-pressure variation were neither needed nor provided. Static pressure taps for time-averaged measurements were placed along the line of symmetry for the two-dimensional system, and along the external walls for both axisymmetric[9] and two-dimensional channels.

**Table 3 Configurations tested for diagnostic two-dimensional data acquisition[a]**

| $N_{e_{II}}^*/H$ | 4, mm | 5, mm | 6, mm | 7, mm | 8, mm | 9, mm | 10, mm |
|---|---|---|---|---|---|---|---|
| 18 (mm) | 1[b] | 5 | | | | | |
| 19 | 2 | 6 | 10 | | | | |
| 20 | 3 | 7 | 11 | 15 | 20 | 25 | |
| 21 | 4 | 8 | 12 | 16 | 21 | 26 | 30 |
| 22 | | 9 | 13 | 17 | 22 | 27 | 31 |
| 23 | | | 14 | 18 | 23 | 28 | 32 |
| 24 | | | | 19 | 24 | 29 | 33 |
| 25 | | | | | | | 34 |
| Open[c] | 35 | 36 | 37 | 38 | 39 | 40 | 41 |

[a]All configurations tested at $L = 76$ mm, 101 mm, $M_{e_I} = 1.61$ (nominal); all configurations tested at $P_{o_I} = 15, 25, 35, 45, 55$ psig.
[b]Number assigned for the configuration case.
[c]Open means no constriction was used.

All of the experiments were carried out at the continuous-flow facilities of the Department of Mechanical and Industrial Engineering Gas Dynamics Laboratory. These continuous-flow stands allow for accurate control over a wide range of stagnation chamber pressures. The test stands include attachments to an illuminated manometer bank where static pressures are displayed for photographic recording.

A high-frequency transducer was placed in the base region where the pressure fluctuations are most significant, as is emphasized in the analysis. Fast Fourier analysis of the transducer signals on selected parametric combinations was performed to obtain power spectra information. Base pressure spectral analysis permitted the detection of weak or incipient wave formations, whose traces on the oscilloscope do not show clearly strict periodicity. A data acquisition flow diagram is presented in Fig. 11. The computer systems used for data processing and reduction included HP 9800, Cyber 175, and PDP 11-34 systems. Table 3 lists the test cases for the two-dimensional experiments.

#### Channel and Base Pressure History Experiments

Figure 12 offers an overall view of the two-dimensional test section in which one can see the configuration and the transducer tap locations. A single transducer tap is used for the permanent placement of the base area transducer. The transducer taps are 0.25 in. apart and the "zero-volume" transducer mount is bolted onto this plate at the desired test location.

The locations of pressure taps used are marked on the figure by a letter code. Only one set of geometrical and operational parameters was tested. Table 4 presents the actual transducer locations along with the rest of the pertinent information.

An oscilloscope coupled with an amplifier and transducer excitation voltage supply displayed the pressure signals. Simultaneous recording of more than two transducers was not possible, which led to the placement of one transducer permanently at the base region to serve as phase reference in the cycle. The signals were then photographed for further digitization and data processing. Data reduction and plotting was achieved by computer programs based on the Cyber 175 and HP 9800 systems. The results from these tests are presented in Tables 5 and 6.

## V. Comparison of Theoretical and Experimental Results

A large body of experimental data[9] is available for examination with the main objective of finding whether a highly simplified theory can provide useful information on the following practical questions: 1) under what conditions will nonsteady near-cyclic operation be expected, 2) if nonsteady operation is occurring, what pressure peaks will be anticipated, and 3) can cyclic frequencies be predicted.

Although the development of computer programs has made it possible to deal in principle with all of the geometrical and operational parameters germaine to the problem, only a few, but typical cases have been selected here for the purpose of comparison.

In addressing item 1 above, Fig. 6 shows that the geometrical parameters for producing nonsteady operation can be predicted (additional restrictions are low-speed motion of the rocket $V_R < S$ and $L$ large enough to allow plume attachment ahead of the channel exit restriction).

With respect to item 2, Fig. 13a indicates that the static pressure peaks predicted by the theory are verified to occur in a region slightly upstream of the channel restriction (see Fig.

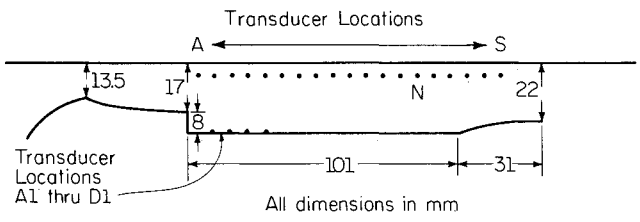


**Fig. 12 Two-dimensional configuration for channel pressure history acquisition showing dimensions and transducer locations.**

**Table 4 Transducer locations in the two-dimensional test configuration[a]**

| Transducer location | Distance from nozzle exit, mm | Transducer location | Distance from nozzle exit, mm |
|---|---|---|---|
| Locations 5 mm from symmetry line | | | |
| A | 4.0 | K | 67.5 |
| B | 10.35 | L | 73.85 |
| C | 16.7 | M | 80.2 |
| D | 23.05 | N | 86.55 |
| E | 29.14 | O | 92.9 |
| F | 37.75 | P | 99.25 |
| G | 42.1 | Q | 105.6 |
| H | 48.25 | R | 111.95 |
| I | 54.8 | S | 118.3 |
| J | 61.15 | | |

Locations along backstep wall

| Transducer location | Distance from backstep (mm) |
|---|---|
| A1 | 8.4 |
| B1 | 15.4 |
| C1 | 22.5 |
| D1 | 30.1 |

[a]Test configuration: $M_{e_I} = 1.585$ (nominal 1.611), $h = 8$ mm, $H^*_{e_{II}} = 22$ mm, $L = 101$ mm, $P_{o_I} = 74.5$ psia, $H_{e_I} = 19$ mm.

**Table 5 Experimental results for test configurations where nonsteady operation occurred in two-dimensional diagnostic experiments; $L = 76$ mm (see Fig. 4)**

| $H$, mm | $A^*_I/A^*_{II}$ | $H^*_{e_{II}}/D$ | $P_{Atm}/P_{o_I}$ | $P_b/P_{e_I}$/Avg[a] | $f$, Hz |
|---|---|---|---|---|---|
| 10 | 0.587 | 0.85 | 0.3 | 0.963 | 230 |
| | 0.587 | 0.85 | 0.25 | 0.90 | 234 |
| | 0.587 | 0.85 | 0.215 | 0.96 | 213 |
| | 0.614 | 0.815 | 0.25 | 1.02 | 165 |
| | 0.614 | 0.815 | 0.215 | 0.99 | 160 |
| 9 | 0.587 | 0.885 | 0.3 | 0.796 | 235 |
| | 0.587 | 0.885 | 0.25 | 0.776 | 250 |
| | 0.587 | 0.885 | 0.215 | 0.765 | 245 |
| | 0.614 | 0.846 | 0.3 | 0.83 | 240 |
| | 0.614 | 0.846 | 0.25 | 0.83 | 222 |
| | 0.614 | 0.846 | 0.215 | 0.813 | 217 |
| 8 | 0.587 | 0.92 | 0.375 | 1.03 | 210 |
| | 0.587 | 0.92 | 0.3 | 0.535 | 180 |
| | 0.587 | 0.92 | 0.25 | 0.507 | 166 |
| | 0.587 | 0.92 | 0.215 | 0.498 | 178 |
| | 0.614 | 0.88 | 0.3 | 0.601 | 188 |
| | 0.614 | 0.88 | 0.25 | 0.573 | 182 |
| | 0.614 | 0.88 | 0.215 | 0.570 | 190 |
| 7 | 0.587 | 0.96 | 0.375 | 0.605 | 177 |
| | 0.614 | 0.916 | 0.3 | 0.553 | 205 |
| | 0.614 | 0.916 | 0.25 | 0.516 | 195 |
| | 0.614 | 0.916 | 0.215 | 0.508 | 208 |
| 6 | 0.614 | 0.956 | 0.3 | 0.535 | 181 |
| | 0.614 | 0.956 | 0.25 | 0.507 | 181 |
| | 0.614 | 0.956 | 0.215 | 0.488 | 200 |
| 5 | 0.643 | 0.9546 | 0.375 | – – | 185 |
| | 0.675 | 0.909 | 0.25 | – – | 186 |
| | 0.675 | 0.909 | 0.215 | – – | 166 |

[a]As obtained from manometer readings.

**Table 6 Experimental results for test configurations where nonsteady operation occurred in two-dimensional diagnostic experiments; $L$ = 101 mm (see Fig. 5)**

| $H$, mm | $A_I^*/A_{II}^*$ | $He_{II}^*/D$ | $P_{Atm}/P_{o_I}$ | $P_b/P_{e_I}$/Avg[a] | $f$, Hz |
|---|---|---|---|---|---|
| 10 | 0.587 | 0.85 | 0.3 | 0.7278 | 143 |
| | 0.614 | 0.815 | 0.3 | 0.87 | 156 |
| | 0.614 | 0.815 | 0.25 | 0.839 | 161 |
| | 0.614 | 0.815 | 0.215 | 0.838 | 173 |
| 9 | 0.587 | 0.885 | 0.375 | 0.7638 | 142 |
| | 0.614 | 0.846 | 0.3 | 0.7695 | 156 |
| | 0.614 | 0.846 | 0.25 | 0.7465 | 166 |
| | 0.614 | 0.846 | 0.215 | 0.7408 | 166 |
| | 0.614 | 0.846 | 0.1875 | 0.7317 | 166 |
| 8 | 0.563 | 0.96 | 0.375 | 0.624 | 278 |
| | 0.587 | 0.92 | 0.375 | 0.745 | 172 |
| | 0.614 | 0.88 | 0.3 | 0.782 | 162 |
| | 0.614 | 0.88 | 0.25 | 0.776 | 160 |
| | 0.614 | 0.88 | 0.215 | 0.761 | 166 |
| 7 | 0.643 | 0.875 | 0.375 | 0.971 | 125 |
| | 0.643 | 0.875 | 0.3 | 0.779 | 155 |
| | 0.643 | 0.875 | 0.25 | 0.7604 | 155 |
| | 0.643 | 0.875 | 0.215 | 0.7540 | 160 |
| | 0.643 | 0.875 | 0.1875 | 0.743 | 155 |
| 6 | 0.614 | 0.913 | 0.375 | 0.7378 | 155 |
| | 0.653 | 0.956 | 0.3 | 0.882 | 133 |
| | 0.643 | 0.913 | 0.25 | 0.879 | 123 |
| | 0.643 | 0.913 | 0.215 | 0.866 | 120 |
| 5 | 0.643 | 0.9545 | 0.375 | 0.904 | 108 |
| | 0.643 | 0.9545 | 0.3 | 0.868 | 136 |
| | 0.643 | 0.9545 | 0.25 | 0.841 | 138 |
| | 0.643 | 0.9545 | 0.215 | 0.845 | 142 |

[a]As obtained from manometer readings.

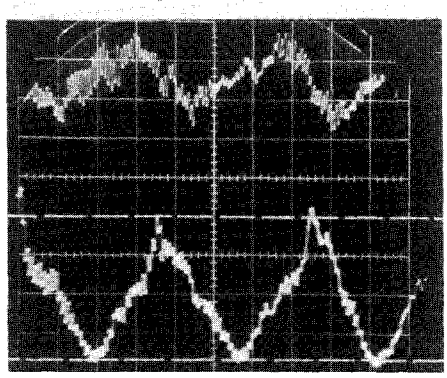


**Fig. 13a Oscilloscope traces of base pressure oscillations (lower trace) and pressure oscillations at location $N$ (upper trace) in the two-dimensional channel (see Fig. 7).**

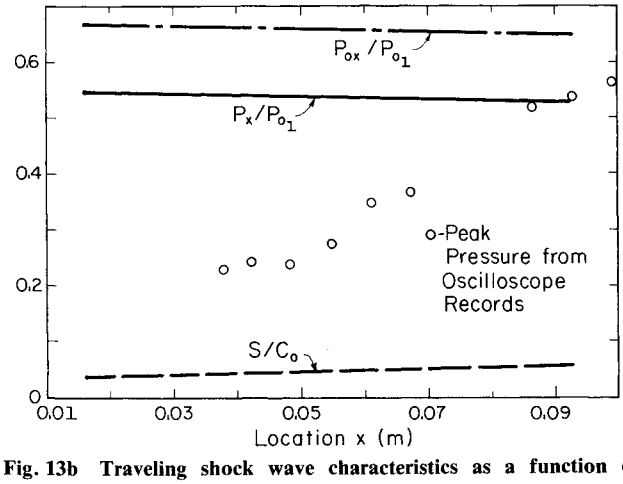


**Fig. 13b Traveling shock wave characteristics as a function of location in channel.**

13b). With reference to Fig. 1, it is easy to understand why the theoretical assumption of a single normal shock wave does not hold for the region of complex oblique-wave interactions in the upstream portion of the channel, yet produces reasonable results once the flow pattern becomes nearly uniform and entirely subsonic. The prediction of cyclic frequencies (item no. 3) is rendered difficult by the overlapping nature of events treated separately by the theory. Yet, for the selected cases ($L_1$ = 0.10 m and $L_2$ = 0.076 m, Tables 5 and 6), it is gratifying to observe that an estimate based on Eq. (11) yields the reasonable results shown below:

| | Theory | Measured |
|---|---|---|
| $L_1 = 0.101$ | 167.6 | 162.7 ± 2.5 |
| $L_2 = 0.076$ | 193.53 | 186.7 ± 3.4 |

## VI. Conclusions

Supported by qualitative studies using the hydraulic analogy and high-speed air experiments with two-dimensional (and axisymmetric) channel models, component flows mechanisms have been delineated subjected to theoretical analysis and synthesized into an overall operational model. It has been shown that the problem of nonsteady rocket plume-wall interactions during initial launch phases can be attacked by highly simplified theoretical concepts to yield useful information on peak pressures and cycle frequencies.

## Acknowledgment

This work was supported in part by the U.S. Army Research Office, Research Grant DAAG 29-79-C-0184.

## References

[1]Page, R. H., "A Review of Component Analysis of Base Pressure for Turbulent Flow," *Proceedings of the Tenth International Symposium on Space Technology and Science*, Tokyo, Japan, Sept. 1974.

[2]Alpinieri, L. J. and Adams, R. M., "Flow Separation Due to Jet Pluming," *AIAA Journal*, Vol. 4, Oct. 1966, pp. 1865-1866.

[3]Batson, J. L. and Bertin, J. J., "Rocket Exhaust Flow in Tube Launchers," *Journal of Spacecraft and Rockets*, Vol. 11, Nov. 1974, pp. 739-790.

[4]Rockwell, O., "Oscillations of Impinging Shear Layers," *AIAA Journal*, Vol. 21, May 1983, pp. 645-664.

[5]Meier, G. E. A., Grabitz, G., Jungowski, W. M., Witczak, K. J., and Anderson, J. S., "Oscillations of the Supersonic Flow Downstream of an Abrupt Increase in Duct Cross-Section," Max-Planck Inst., Goettingen, Federal Republic of Germany, Rept. 65, 1978.

[6]Jungowski, W. M., "Some Self-Induced Supersonic Flow Oscillation," *Progress in Aerospace Science*, Vol. 18, Jan. 1978, pp. 151-176.

[7]Chen, C. P., Sajben, M., and Kroutil, J. C., "Shock-Wave Oscillations in a Transonic Diffuser Flow," *AIAA Journal*, Vol. 17, Oct. 1979, pp. 1076-1083.

[8]Bogar, T. J., Sajben, M., and Kroutil, J. C., "Characteristic Frequencies of Transonic Diffuser Flow Oscillations," *AIAA Journal*, Vol. 21, Sept. 1983, pp. 1232-1240.

[9]Marongiu, M., "Mechanisms Controlling Non-Steady Plumes-Wall Interactions in Rocket Launch Tubes," Ph.D. Dissertation, Dept. of Mechanical and Industrial Engineering, Univ. of Illinois at Urbana-Champaign, IL, July 1985.

[10]Korst, H. H. and Bertin, J. J., "The Analysis of Secondary Flows for Tube-Launched Rocket Configurations," *Journal of Spacecraft and Rockets*, Vol. 20, Jan.-Feb. 1983, pp. 35-42.

[11]Ihrig, H. K. Jr. and Korst, H. H., "Quasi-Steady Aspects of the Adjustment of Separated Flow Regions to Transient External Flows," *AIAA Journal*, Vol. 1, 1963, pp. 934-936.

[12]Carriere, P., Sirieix, M., and Delery, J., "Methodes de Calcule des Ecoulements Turbulents Decollés en Supersonique," *Progress in Aerospace Sciences*, Vol. 16, 1975, pp. 385-429.

[13]Page, R. H., Hill, W. G., Jr., and Kessler, T. J., "Reattachment of Two-Dimensional Supersonic Turbulent Flows," American Society of Mechanical Engineers Paper 67-FE-20, May 1967.

[14]Chapman, D. R. and Korst, H. H., "Theory of Base Pressures in Transonic and Supersonic Flow," *Journal of Applied Mechanics*, Vol. 24, 1957, p. 484.